Ground Reference Points in Legged Locomotion: Definitions, Biological Trajectories and Control Implications.

Article *in* The International Journal of Robotics Research · January 2005

Source: DBLP

CITATIONS
137

READS
117

3 authors:

Marko B. Popovic
Worcester Polytechnic Institute
36 PUBLICATIONS **1,096** CITATIONS

SEE PROFILE

Ambarish Goswami
Intuitive Surgical
75 PUBLICATIONS **3,969** CITATIONS

SEE PROFILE

Hugh Herr
Massachusetts Institute of Technology
128 PUBLICATIONS **6,806** CITATIONS

SEE PROFILE

Marko B. Popovic
The Media Laboratory
Massachusetts Institute of Technology
Cambridge, MA 02139-4307, USA

Ambarish Goswami
Honda Research Institute
Mountain View, CA 94041, USA

Hugh Herr
MIT Media Laboratory
MIT-Harvard Division of Health
Sciences and Technology
Spaulding Rehabilitation Hospital,
Harvard Medical School
Cambridge, MA 02139-4307, USA
hherr@media.mit.edu

Ground Reference Points in Legged Locomotion: Definitions, Biological Trajectories and Control Implications

Abstract

The zero moment point (ZMP), foot rotation indicator (FRI) and centroidal moment pivot (CMP) are important ground reference points used for motion identification and control in biomechanics and legged robotics. In this paper, we study these reference points for normal human walking, and discuss their applicability in legged machine control. Since the FRI was proposed as an indicator of foot rotation, we hypothesize that the FRI will closely track the ZMP in early single support when the foot remains flat on the ground, but will then significantly diverge from the ZMP in late single support as the foot rolls during heel-off. Additionally, since spin angular momentum has been shown to remain small throughout the walking cycle, we hypothesize that the CMP will never leave the ground support base throughout the entire gait cycle, closely tracking the ZMP. We test these hypotheses using a morphologically realistic human model and kinetic and kinematic gait data measured from ten human subjects walking at self-selected speeds. We find that the mean separation distance between the FRI and ZMP during heel-off is within the accuracy of their measurement (0.1% of foot length). Thus, the FRI point is determined not to be an adequate measure of foot rotational acceleration and a modified FRI point is proposed. Finally, we find that the CMP never leaves the ground support base, and the mean separation distance between the CMP and ZMP is small (14% of foot length), highlighting how closely the human body regulates spin angular momentum in level ground walking.

The International Journal of Robotics Research
Vol. 24, No. 10, October 2005, pp. xxx-xxx,
DOI: 10.1177/0278364905058363

Figures 1 and 3–9 appear in color online: http://jrp.sagepub.com

KEY WORDS—legged locomotion, control, biomechanics, human, zero moment point, center of pressure, foot rotation indicator, centroidal moment pivot

1. Nomenclature

$\vec{a}_i$ = body segment i center of mass acceleration
α = parameter used for optimization of human model mass parameters
D = relative mass distribution described by a 16-component vector
D_A = average relative mass distribution (Winter 1990)
D_R = resulting relative mass distribution
D_S = subject specific relative mass distribution obtained by equal density assumption
D_S^i = relative mass of the ith link
$\vec{F}$ = net force acting on a whole body (in free fall $F_x = F_y = 0$, $F_z = -Mg$)
$\vec{F}_{ankle}$ = net force at the stance foot ankle joint exerted from the rest of the body
$\vec{F}_{G.R.}$ = ground reaction force
$F_{G.R.\perp}$ = component of the ground reaction force normal to the surface
$\vec{F}_{R.}$ = reaction force (general surface)
F_x^{moment} = net zero force in x-direction corresponding to the moment balance strategy
$F_x^{zero-moment}$ = net zero force in x-direction corresponding to the zero-moment balance strategy
g = gravitational constant (9.81 m s^{-2})

$\vec{g}$ = gravitational vector $(-g \cdot \vec{e}_Z)$
$\overleftrightarrow{I}_i$ = body segment i inertia tensor about the link's center of mass
$\overleftrightarrow{I}_i(\vec{r}_{CM})$ = time-dependent segment i moment of inertia tensor about the center of mass
$\overleftrightarrow{I}(\vec{r}_{CM})$ = time-dependent whole-body moment of inertia tensor about the center of mass
$\vec{L}^{foot}(\vec{r}_F)$ = angular momentum of the foot about some point F
$\vec{L}^{foot}(\vec{r}_{FRI})$ = angular momentum of the foot about the foot rotation indicator point
$\vec{L}^{foot}(\vec{r}_{\text{mod}.FRI})$ = angular momentum of the foot about the modified foot rotation indicator point
$\vec{L}_{des.}(\vec{r}_{CM})$ = desired whole-body angular momentum
l_{foot} = length of the foot
M = body mass
m_{foot} = mass of the foot
m_i = body segment i mass
$\vec{n}_\perp$ = unit vector normal to the surface and pointing away from the ground
P_A = average distribution of link densities (Winter 1990)
$P(\alpha)$ = density profile described by the 16-component vector
$P^i(\alpha) = M\ D^i(\alpha) \big/ V^i$ = density of the ith link
$\vec{p}_{foot}$ = linear momentum of the foot's center of mass
$\dot{\vec{p}}_{foot}$ = net force acting on the foot
$p(\vec{r})$ = pressure at location $\vec{r}$
$\vec{r}_{ankle}$ = stance foot ankle joint center
$\vec{r}_{CM}$ = body center of mass
$\vec{r}_{CMP}$ = centroidal moment pivot point
$\vec{r}_{foot}$ = stance foot center of mass
$\vec{r}_{FRI}$ = foot rotation indicator point
$\vec{r}_i$ = body segment i center of mass
$\vec{r}_{\text{mod}.FRI}$ = modified foot rotation indicator point
$\vec{r}_{ZMP}$ = zero moment point
t = time
$\vec{\tau}\ (\vec{r}_{ZMP})\,|_{horizontal}$ = horizontal component (orthogonal to gravity vector) of the net moment about the zero moment point
$\vec{\tau}_{ankle}$ = net torque at the stance foot ankle joint exerted from the rest of the body
$\vec{\tau}_{des.}(\vec{r}_{CM})$ = desired target whole-body moment about the center of mass
$\vec{\tau}_{G.R.}(0)|_{horizontal}$ = resulting moment exerted from the ground on the body about the origin of the lab reference frame
$\vec{\tau}_{G.R.}(\vec{r}_{ZMP})|_{horizontal}$ = horizontal component (orthogonal to gravity vector) of the moment of ground reaction force about the zero moment point
$\vec{\tau}_{inertia+gravity}(\vec{r}_{ZMP})|_{horizontal}$ = horizontal component (orthogonal to gravity vector) of the moment due to inertial and gravitational forces about the zero moment point
$\vec{\tau}|_{||}$ = component of the whole-body moment parallel to the flat surface (i.e., $\vec{\tau}|_{||} \cdot \vec{n}_\perp = 0$)
$\vec{\theta}$ = time-dependent whole-body angular excursion vector
$\vec{\theta}_{des.}$ = desired target whole-body angular excursion
$\ddot{\vec{\theta}}_{des.}$ = desired target whole-body angular acceleration
$\vec{v}$ = time-dependent whole-body center of mass velocity (error in paper)
V^i = volume of the ith link
$\vec{\omega}$ = time-dependent whole-body angular velocity vector
$\vec{\omega}_i$ = body segment i angular velocity
$x = {}^{2a_{foot}}\!/_{g}$ = relative heel acceleration
x_{peak} = peak relative heel acceleration
$\ddot{z}_{CM}$ = body center of mass acceleration in the vertical direction (in free fall $\ddot{z}_{CM} = -g$)

2. Introduction

Legged robotics has witnessed many impressive advances in the last several decades, from animal-like, hopping robots in the 1980s (Raibert 1986) to walking humanoid robots at the turn of the century (Hirai 1997; Hirai et al. 1998; Chew, Pratt, and Pratt 1999; Yamaguchi et al. 1999; Kagami et al. 2000). Although the field has witnessed tremendous progress, legged machines that demonstrate biologically realistic movement patterns and behaviors have not yet been offered, due in part to limitations in control technique (Schaal 1999; Pratt 2002). An example is the Honda robot, a remarkable autonomous humanoid that walks across level surfaces and ascends and descends stairs (Hirai 1997; Hirai et al. 1998). The stability of the robot is obtained using a control design that requires the robot to accurately track precisely calculated joint trajectories. In distinction, for many movement tasks, animals and humans control limb impedance, allowing for a more robust handling of unexpected disturbances (Pratt 2002).

The development of animal-like and human-like robots that mimic the kinematics and kinetics of their biological counterparts, quantitatively or qualitatively, is indeed a formidable task. Humans, for example, are capable of performing numerous dynamical movements in a wide variety of complex and novel environments while robustly rejecting a large spectrum of disturbances. Given limitations on computational capacity, real-time trajectory planning in joint space does not seem feasible using optimization strategies with moderately long future time horizons. Subsequently, for the diversity of biological motor tasks to be represented in a robot's movement repertoire, the control problem has to be restated using a lower-dimensional representation (Full and Koditschek 1999). However, independent of the specific architecture that achieves that reduction in dimension, biomechanical motion characteristics have to be identified and appropriately addressed.

There are several ground reference points used for motion identification and control in biomechanics and legged robotics. The locations of these reference points relative to each other, and relative to the ground support area, provide important local and sometimes global characteristics of whole-body movement, serving as benchmarks for either physical or

desired movement patterns. The zero moment point (ZMP), first discussed by Elftman[1] (1938) for the study of human biomechanics, has only more recently been used in the context of legged machine control (Vukobratovic and Juricic 1969; Vukobratovic and Stepanenko 1973; Takanishi et al. 1985; Yamaguchi, Takanishi and Kato 1993; Hirai 1997; Hirai et al. 1998). In addition to this standard reference point, Goswami (1999) introduced the foot rotation indicator (FRI), a ground reference point that provides information on stance-foot angular accelerations when only one foot is on the ground. Since its introduction, the FRI has been used in legged robotic controllers to determine whether the stance foot is flat on the ground or rolling with angular acceleration during single support (Wollherr et al. 2003; Hofmann et al. 2004; Popovic, Englehart and Herr 2004; Choi and Grizzle 2005). The centroidal moment pivot (CMP) is yet another ground reference point recently introduced in the literature (Herr, Hofmann, and Popovic 2003; Hofmann, 2003; Goswami and Kallem 2004; Popovic, Hofmann, and Herr 2004a). When the CMP corresponds with the ZMP, the ground reaction force passes directly through the center of mass (CM) of the body, satisfying a zero moment or rotational equilibrium condition. Hence, the departure of the CMP from the ZMP is an indication of non-zero CM body moments, causing variations in whole-body, spin angular momentum.

In this paper we study the ZMP, FRI, and CMP ground reference points. Using a consistent mathematical notation, we define and compare the ground points in Section 3 and outline the various methodologies that can be employed in their estimation. In Section 4, we analyze the ZMP, FRI, and CMP trajectories for level-ground, steady-state human walking, and in Section 5, we conclude the paper with a discussion of the significance of the ground reference points to legged robotic control systems.

In Section 4, two key hypotheses are tested regarding the nature of the ground reference points in level-ground, steady-state human walking. As known from gait observations, the stance foot rolls and undergoes angular accelerations late in the single support phase of walking, as the heel lifts from the walking surface during powered plantar flexion (Rose and Gamble 1994). In distinction, throughout the controlled dorsiflexion phase of single support, the foot does not roll but remains flat on the ground. Hence, we hypothesize that the FRI trajectory will closely track the ZMP trajectory throughout the controlled dorsiflexion phase of single support, but will then significantly diverge from the ZMP trajectory, leaving the ground support base during powered plantar flexion. In addition to the FRI reference trajectory, we also study the character of the CMP trajectory in human walking. Because recent biomechanical investigations have shown that total spin angular momentum is highly regulated throughout the walking cycle (Popovic, Gu, and Herr 2002; Gu 2003; Herr, Whiteley and Childress 2003; Herr and Popovic 2004; Popovic, Hofmann, and Herr 2004a), we hypothesize that the CMP trajectory will never leave the ground support base throughout the entire walking gait cycle, closely tracking the ZMP trajectory throughout the single and double support phases of gait. We test both the FRI and CMP hypotheses using a morphologically realistic human model and kinetic and kinematic gait data measured from ten human subjects walking at self-selected walking speeds.

1. Although Borelli (1680) discussed the concept of the ZMP for the case of static equilibrium, it was Elftman (1938) who introduced the point for the more general dynamic case. Elftman named the specified point the "position of the force" and built the first ground force plate for its measurement.

3. ZMP, FRI, and CMP Reference Points: Definitions and Comparisons

In this section, we define the ground reference points: ZMP, FRI, and CMP. Although the reference points have been defined previously in the literature, we define and compare them here using a consistent terminology and mathematical notation.

In this paper, we adopt a notation by which $\vec{\tau}(\vec{r}_A)$ symbolizes the total moment acting on a body about point $\vec{r}_A$. For example, $\vec{\tau}(0)$ symbolizes a moment calculated at the origin of a coordinate frame. This notation stresses the fact that a moment of force acting on a body changes depending on the point about which it is calculated. In addition to the point about which the moment is calculated, we also designate the force used in the moment calculation. For example, if we consider only the moment due to the ground reaction force acting on a body, we specify this with the subscript $G.R.$, i.e., $\vec{\tau}_{G.R.}(\vec{r}_A)$. Also, in this paper when we consider only a moment that acts on a particular body segment, or group of segments, we specify that moment using the segment's name in the superscript, e.g., $\vec{\tau}^{foot}(\vec{r}_A)$. In addition, in this paper, we often refer to the ground support base (GSB) to describe the foot–ground interaction. The GSB is the actual foot–ground contact surface when only one foot is in contact with the ground, or the convex hull of the two or more discrete contact surfaces when two or more feet are in contact with the ground, respectively. Finally, the ground support envelope is used to denote the actual boundary of the foot when the entire foot is flat on the contact surface, or the actual boundary of the convex hull when two or more feet are flat on the contact surface. In contrast to the GSB, the ground support envelope is not time varying even in the presence of foot rotational accelerations or rolling.

3.1. Zero Moment Point

In the book *On the Movement of Animals*, Borelli (1680) discussed a biomechanical point that he called the support point, a ground reference location where the resultant ground reaction force acts in the case of static equilibrium. Much later, Elftman (1938) defined a more general "position of the force" for both static and dynamic cases, and he built the first ground force

plate for its measurement. Following this work, Vukobratovic and Juricic (1969) revisited Elftman's point and expanded its definition and applicability to legged machine control. They defined how the point can be computed from legged system state and mass distribution, allowing a robotic control system to anticipate future ground–foot interactions from desired body kinematics. For the application of robotic control, they renamed Elftman's point the ZMP.

Although for flat horizontal ground surfaces the ZMP is equal to the center of pressure, the points are distinct for irregular ground surfaces. In Appendix A, we properly define these ground points, and prove their equivalence for horizontal ground surfaces, and their uniqueness for more complex contact topologies.

Vukobratovic and Juricic (1969) defined the ZMP as the "point of resulting reaction forces at the contact surface between the extremity and the ground". The ZMP, $\vec{r}_{ZMP}$, therefore may be defined as the point on the ground surface about which the horizontal component of the moment of ground reaction force is zero (Arakawa and Fukuda 1997; Vukobratovic and Borovac 2004), or

$$\vec{\tau}_{G.R.}(\vec{r}_{ZMP})|_{horizontal} = 0. \tag{1}$$

Equation (1) means that the resulting moment of force exerted from the ground on the body about the ZMP is always vertical, or parallel to $\vec{g}$. The ZMP may also be defined as the point on the ground at which the net moment due to inertial and gravitational forces has no component along the horizontal axes (Hirai et al. 1998; Dasgupta and Nakamura 1999; Vukobratovic and Borovac 2004), or

$$\vec{\tau}_{inertia+gravity}(\vec{r}_{ZMP})|_{horizontal} = 0. \tag{2}$$

Proof that these two definitions are in fact equal may be found in Goswami (1999) and more recently in Sardain and Bessonet (2004).

Following from eq. (1), if there are no external forces except the ground reaction force and gravity, the horizontal component of the moment that gravity creates about the ZMP is equal to the horizontal component of the total body moment about the ZMP, $\vec{\tau}(\vec{r}_{ZMP})|_{horizontal}$, or

$$\vec{\tau}\ (\vec{r}_{ZMP})\,|_{horizontal} = \left[(\vec{r}_{CM} - \vec{r}_{ZMP}) \times M\vec{g}\right]_{horizontal} \tag{3}$$

where $\vec{r}_{CM}$ is the CM and M is the total body mass. Using detailed information of body segment dynamics, this can be rewritten as

$$\sum_{i=1}^{N}\left[(\vec{r}_i - \vec{r}_{ZMP}) \times m_i\vec{a}_i + \frac{\mathrm{d}(\overleftrightarrow{I}_i\vec{\omega}_i)}{\mathrm{d}t}\right]_{horizontal} = \left[(\vec{r}_{CM} - \vec{r}_{ZMP}) \times M\vec{g}\right]_{horizontal}, \tag{4}$$

where $\vec{r}_i$ is the CM of the ith link, m_i is the mass of the ith link, $\vec{a}_i$ is the linear acceleration of the ith link CM, $\overleftrightarrow{I}_i$ is the inertia tensor of the ith link about the link's CM, and $\vec{\omega}_i$ is the angular velocity of the ith link. Equation (4) is a system of two equations with two unknowns, x_{ZMP} and y_{ZMP}, which can be solved to give

$$x_{ZMP} = -\frac{\sum_{i=1}^{N}\left\{\vec{r}_i \times m_i(\vec{a}_i - \vec{g}) + \left[\mathrm{d}\left(\overleftrightarrow{I}_i\vec{\omega}_i\right)/\mathrm{d}t\right]\right\}_Y}{M\left(\ddot{Z}_{CM} + g\right)} \tag{5}$$

and

$$y_{ZMP} = \frac{\sum_{i=1}^{N}\left\{\vec{r}_i \times m_i(\vec{a}_i - \vec{g}) + \left[\mathrm{d}\left(\overleftrightarrow{I}_i\vec{\omega}_i\right)/\mathrm{d}t\right]\right\}_X}{M\left(\ddot{Z}_{CM} + g\right)}.$$

Given full body kinematics and the mass distribution of a legged system, eq. (5) can be used to reconstruct the ZMP trajectory. Alternatively, at a particular instant in time, eq. (5) can be employed as a constraint equation for deciding joint accelerations consistent with a desired ZMP position, as discussed by Kondak and Hommel (2003).

Finally, the ZMP as a function of the CM position, net CM force ($\vec{F} = M\vec{a}_{CM}$), and net moment about the CM can be expressed as

$$x_{ZMP} = x_{CM} - \frac{F_x}{F_z + Mg}z_{CM} - \frac{\tau_y(\vec{r}_{CM})}{F_z + Mg} \tag{6}$$

and

$$y_{ZMP} = y_{CM} - \frac{F_y}{F_z + Mg}z_{CM} + \frac{\tau_x(\vec{r}_{CM})}{F_z + Mg}.$$

As emphasized in Figure 1, the most important notion of the ZMP quantity, applicable for both single and multileg ground support phases, is that it resolves the ground reaction force distribution to a single point. However, one needs to be careful to use this point in an appropriate manner. Most notably, both the vertical component of moment and the CM work performed by the ground reaction force cannot be computed solely on the bases of the ZMP trajectory and the resulting ground reaction force vector. For example, the resultant horizontal ground reaction force could be zero while the vertical component of moment and/or the work performed by the ground reaction force could be non-zero. Consider a legged posture in which the following conditions are satisfied: (1) the ZMP is located just beneath the CM; (2) the horizontal ground reaction force field is tangent to a circle centered about the ZMP; (3) the horizontal ground reaction force magnitude is a function of only radial distance. In this situation, shown in Figure 2, the net horizontal force is zero, but the net moment is non-zero. Another example is two particles of equal mass subject to two forces equal in magnitude but acting in opposite directions; while the net force is zero and the CM is at rest, the particles

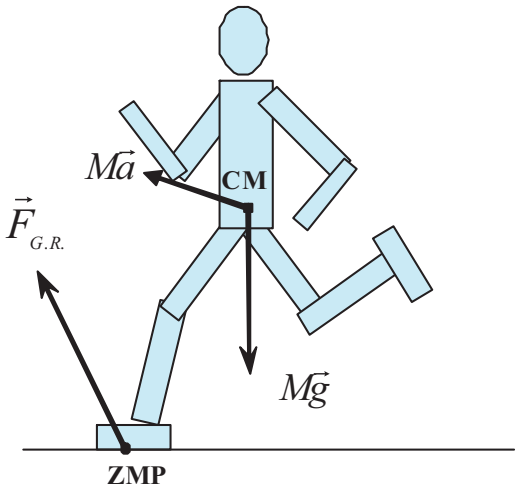

Fig. 1. Zero moment point. The ZMP is where the ground reaction force acts whereas the CM point is where inertia and the force of gravity originate.

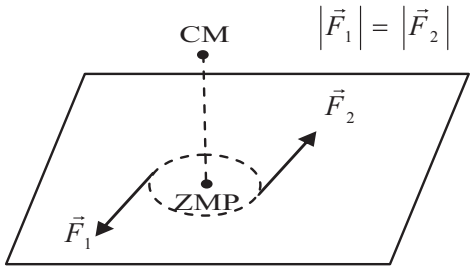

Fig. 2. A legged posture is shown in which the ZMP is located just beneath the CM, the horizontal ground reaction force field is tangent to a circle centered about the ZMP, and the horizontal ground reaction force magnitude is a function of only radial distance. In this case, the net horizontal force is zero, but the net moment is non-zero. Thus, both the vertical component of moment and the CM work performed by the ground reaction force cannot be computed solely on the bases of the ZMP trajectory and the resulting ground reaction force vector.

are moving and the work conducted by the external forces is non-zero. In other words, neither $\delta W_{G.R.} = \vec{F}_{G.R.}\delta\vec{r}_{ZMP}$ nor $\delta W_{G.R.} = \vec{F}_{G.R.}\delta\vec{r}_{CM}$ is a permissible expression for the work performed by the ground reaction force.

3.2. Foot Rotation Indicator

3.2.1. Motivation

In legged systems, a loss of rotational equilibrium of the stance foot during single support implies the existence of an unbalanced moment acting on the foot segment, causing foot rotations and movement of the ZMP towards the edge of the footprint boundary. Once the stance foot has rolled to an extreme posture, pushing the ZMP to the very edge of the foot envelope, additional rotational dynamics of the foot, such as different rates of rotational acceleration, are no longer discernible using the ZMP. The FRI point, shown in Figure 3, was introduced by Goswami (1999) in order to specifically address this limitation. Dominant foot rotation has been noted to reflect a loss of balance and an eventual fall in monopods (Lee and Raibert 1991) and bipeds (Arakawa and Fukuda 1997), two classes of legged robots most prone to instabilities. The FRI point extends the concept of the ZMP and quantifies the severity of foot rotational acceleration. A motivation behind its formulation was to achieve a measure of foot rotational acceleration during single support that could be employed by legged control systems as one possible indicator of overall postural instability.

3.2.2. Definition

The FRI point is a point on the foot–ground contact surface, within or outside the support base, where the net ground reaction force would have to act to achieve a zero moment condition about the foot with respect to the FRI point itself. The FRI point coincides with the ZMP when the foot is stationary, and diverges from the ZMP for non-zero rotational foot accelerations.

Consider calculating the rotation of the stance foot during the single support phase in the lab reference frame about some point F on the ground. The rotational dynamical equation for the horizontal moment component is then

$$\left[(\vec{r}_{ZMP} - \vec{r}_F) \times \vec{F}_{G.R.} + (\vec{r}_{foot} - \vec{r}_F) \times m_{foot}\vec{g} + (\vec{r}_{ankle} - \vec{r}_F) \times \vec{F}_{ankle} + \vec{\tau}_{ankle}\right]_{hor} = \left[\frac{d\vec{L}^{foot}(\vec{r}_F)}{dt}\right]_{hor} \quad (7)$$

where $\vec{r}_{foot}$ is the CM of the stance foot, m_{foot} is the mass of the foot, $\vec{r}_{ankle}$ is the ankle joint center at which the force $\vec{F}_{ankle}$ and torque $\vec{\tau}_{ankle}$ are exerted from the rest of the body, and $\vec{L}^{foot}(\vec{r}_F)$ is the angular momentum of the foot about point F.

Now assume the existence of the point FRI for which

$$\vec{\tau}_{G.R.}(\vec{r}_{FRI})\,|_{horizontal} = \left[(r_{ZMP} - \vec{r}_{FRI}) \times \vec{F}_{G.R.}\right]_{horizontal} = \left[\frac{d\vec{L}^{foot}(\vec{r}_{FRI})}{dt}\right]_{horizontal}, \quad (8)$$

and subsequently, from eq. (7),

$$\left[(\vec{r}_{foot} - \vec{r}_{FRI}) \times m_{foot}\vec{g} + (\vec{r}_{ankle} - \vec{r}_{FRI}) \times \vec{F}_{ankle} + \vec{\tau}_{ankle}\right]_{horizontal} = 0. \quad (9)$$

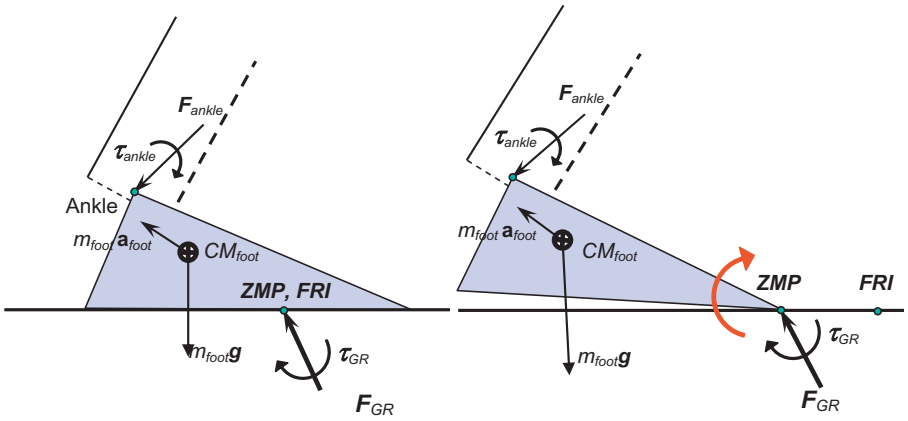

Fig. 3. Foot rotation indicator. The FRI is the point where the ground reaction force would have to act to keep the foot from accelerating. When the foot is stationary, shown in the left figure, the FRI coincides with the ZMP. As the foot starts turning (figure on right), the FRI leaves the support base. Here the distance from the FRI to the ZMP is proportional to the magnitude of the foot moment about the FRI point. Although only two dimensions are depicted in the figure, the FRI definition is applicable to the problem of three-dimensional biped control problems, including foot rotational information for sagittal and coronal planes.

Equations (8) and (9) are two equivalent physical expressions of the FRI point. Clearly, if the stance foot is at rest, then the right-hand side (RHS) of eq. (8) is zero, and the only solution is that the FRI is equal to the ZMP (because $F_{G.R.Z} \neq 0$). However, if the RHS of eq. (8) is not zero, then the FRI differs from the ZMP. While by definition the ZMP point cannot leave the ground support base, the FRI point can. Therefore, the FRI point, in principle, can be employed as an indicator of foot rotational activity for single support movement activities. The non-zero horizontal component of the foot moment is orthogonal to the plane of rotation defined by vectors $(\vec{r}_{ZMP} - \vec{r}_{FRI})$ and $\vec{g}$. By using eq. (8) and the resulting ground reaction force, one could then obtain the magnitude of the foot moment. Note that the definition of the FRI point, defined by eq. (8), does not require a rigid robotic foot; the FRI point could be applied equally well to a compliant, biological or robotic foot.

The FRI point may also be expressed directly from observed foot dynamics. By manipulation of eq. (8), we obtain

$$x_{FRI} = \frac{x_{foot}\ \dot{p}_{Z\ foot} - z_{foot}\ \dot{p}_{X\ foot} - x_{ZMP}\ F_{G.R.Z} - \dot{L}_Y^{foot}(\vec{r}_{foot})}{\dot{p}_{Z\ foot} - F_{G.R.Z}} \tag{10}$$

and

$$y_{FRI} = \frac{y_{foot}\ \dot{p}_{Z\ foot} - z_{foot}\ \dot{p}_{Y\ foot} - y_{ZMP}\ F_{G.R.Z} + \dot{L}_X^{foot}(\vec{r}_{foot})}{\dot{p}_{Z\ foot} - F_{G.R.Z}},$$

where $\vec{p}_{foot}$ denotes the linear momentum of the foot's CM. Alternatively, the FRI can be computed using whole-body kinematic and mass distribution information. The underlying idea here is that the entire legged system can be divided into two portions, one portion consisting of the stance foot and the second portion consisting of the rest of the body. With this division, the RHS of eq. (8) can be rewritten as

$$\left[\frac{\mathrm{d}\vec{L}^{foot}(\vec{r}_{FRI})}{\mathrm{d}t}\right]_{horizontal} = \vec{\tau}(\vec{r}_{FRI})|_{horizontal} - \vec{\tau}^{body-foot}(\vec{r}_{FRI})|_{horizontal}, \tag{11}$$

where $\vec{\tau}^{body-foot}(\vec{r}_{FRI})$ denotes the moment applied on the whole body minus the stance foot moment about the FRI point.

The horizontal moment on the whole body about the FRI point can be expressed as

$$\vec{\tau}(\vec{r}_{FRI})|_{horizontal} = \left[(\vec{r}_{ZMP} - \vec{r}_{FRI}) \times \vec{F}_{G.R.} + (\vec{r}_{CM} - \vec{r}_{FRI}) \times M\vec{g}\right]_{horizontal}. \tag{12}$$

Combining eqs. (8), (11), and (12), we obtain

$$0 = \left[(\vec{r}_{CM} - \vec{r}_{FRI}) \times M\vec{g} - \vec{\tau}^{body-foot}(\vec{r}_{FRI})\right]_{horizontal}. \tag{13}$$

Using detailed information of multibody link dynamics, eq. (13) can be rewritten as

$$0 = \left\{(\vec{r}_{CM} - \vec{r}_{FRI}) \times M\vec{g} - \sum_{i=2}^{N}\left[(\vec{r}_i - \vec{r}_{FRI}) \times m_i\vec{a}_i + \frac{d(\overleftrightarrow{I}_i\vec{\omega}_i)}{dt}\right]\right\}_{horizontal}, \tag{14}$$

where $i = 1$ corresponds to the stance foot. Similar to eq. (4), this is a system of two equations with two unknowns, x_{FRI} and y_{FRI}, which can be easily solved to give

$$x_{FRI} = \quad (15)$$
$$- \frac{\left[-\vec{r}_1 \times m_1\vec{g} + \sum_{i=2}^{N}\left\{\vec{r}_i \times m_i(\vec{a}_i - \vec{g}) + \left[\mathrm{d}\left(\overleftrightarrow{I}_i\vec{\omega}_i\right)/\mathrm{d}t\right]\right\}\right]_Y}{m_1 g + \sum_{i=2}^{N} m_i\left(\ddot{\vec{Z}}_i + g\right)}$$

and

$$y_{FRI} =$$
$$\frac{\left[-\vec{r}_1 \times m_1\vec{g} + \sum_{i=2}^{N}\left\{\vec{r}_i \times m_i(\vec{a}_i - \vec{g}) + \left[\mathrm{d}\left(\overleftrightarrow{I}_i\vec{\omega}_i\right)/\mathrm{d}t\right]\right\}\right]_X}{m_1 g + \sum_{i=2}^{N} m_i\left(\ddot{\vec{Z}}_i + g\right)}.$$

A careful comparison of eqs. (5) and (15) reveals that the FRI point and the ZMP point coincide only if

$$\left[(\vec{r}_1 - \vec{r}_{FRI}) \times m_1\vec{a}_1 + \frac{\mathrm{d}\left(\overleftrightarrow{I}_1\vec{\omega}_1\right)}{\mathrm{d}t}\right]_{horizontal}$$
$$= \left[\frac{\mathrm{d}\vec{L}^{foot}(\vec{r}_{FRI})}{\mathrm{d}t}\right]_{horizontal} = 0. \quad (16)$$

Hence, the distance between the FRI point and the ZMP communicates information about foot rotational dynamics during the single support phase (excluding foot rotations about the vertical axis). When the FRI point coincides with the ZMP point, the foot is stationary. In distinction, when the FRI point diverges from the ZMP, the foot is not stationary but is undergoing non-zero rotational accelerations.

3.3. Centroidal Moment Pivot

3.3.1. Motivation

Biomechanical investigations have determined that for normal, level-ground human walking, spin angular momentum, or the body's angular momentum about the CM, remains small through the gait cycle. Researchers discovered that spin angular momentum about all three spatial axes was highly regulated throughout the entire walking cycle, including both single and double support phases, by observing small moments about the body's CM (Popovic, Gu and Herr 2002) and small spin angular momenta (Herr and Popovic 2004; Popovic, Hofmann, and Herr 2004a). In the latter investigations on spin angular momentum, a morphologically realistic human model and kinematic gait data were used to estimate spin angular momentum at self-selected walking speeds. Walking spin values were then normalized by dividing by body mass, total body height, and walking speed. The resulting dimensionless spin was surprisingly small. Throughout the gait cycle, none of the three spatial components ever exceeded 0.02 dimensionless units.[2]

To determine the effect of the small, but non-zero angular momentum components on whole-body angular excursions in human walking, the whole-body angular velocity vector can be computed, or

$$\vec{\omega}(t) = \overleftrightarrow{I}^{-1}(\vec{r}_{CM}, t)\,\vec{L}(\vec{r}_{CM}, t). \quad (17a)$$

Here, the time-dependent quantity, $\overleftrightarrow{I}(\vec{r}_{CM}, t) = \sum_{i=1}^{N}\overleftrightarrow{I}_i(\vec{r}_{CM}, t)$, is the whole-body inertia tensor about the CM. Subsequently, the whole-body angular velocity vector may be integrated to give the whole-body angular excursion vector, or

$$\vec{\theta}(t) = \int_{-\infty}^{t}\vec{\omega}(t^*)\,\mathrm{d}t^* + C, \quad (17b)$$

where C is an integration constant determined through an analysis of boundary conditions[3] (Popovic, Hofmann, and Herr 2004a). The whole-body angular excursion vector can be accurately viewed as the rotational analog of the CM position vector (i.e., note that analogously $\vec{v} = \dot{\vec{r}}_{CM} = M^{-1}\vec{p}$ and $\vec{r}_{CM}(t) = \int_{-\infty}^{t}\vec{v}_{CM}(t^*)\,\mathrm{d}t^* + D$). In recent biomechanical investigations, angular excursion analyses for level ground human walking showed that the maximum whole-body angular deviations within sagittal (<1°), coronal (<0.2°), and transverse (<2°) planes were negligibly small throughout the walking gait cycle (Herr and Popovic 2005; Popovic, Hofmann and Herr 2004a). These results support the hypothesis that spin angular momentum in human walking is highly regulated by the central nervous system (CNS) so as to keep whole-body angular excursions at a minimum.

According to Newton's laws of motion, a constant spin angular momentum requires that the moments about the CM sum to zero. During the flight phase of running or jumping, angular momentum is perfectly conserved since the dominant external force is gravity acting at the body's CM. However, during the stance period, angular momentum is not necessarily constant because the legs can exert forces on the ground tending

2. Using kinematic data from digitized films (Braune and Fisher 1895), Elftman (1939) estimated spin angular momentum during the single support phase of walking for one human test subject, and found that arm movements during walking decreased the rotation of the body about the vertical axis. Although Elftman did not discuss the overall magnitude of whole-body angular momentum, he observed important body mechanisms for intersegment cancellations of angular momentum.

3. Since the whole-body angular excursion vector defined in eq. (**??**) necessitates a numerical integration of the body's angular velocity vector, its accurate estimate requires a small integration time span and a correspondingly small error in the angular velocity vector.

to accelerate the system (Hinrichs, Cavanagh and Williams 1983; Raibert, 1986; Dapena and McDonald 1989; LeBlanc and Dapena 1996; Gu 2003). Hence, a legged control system must continually modulate moments about the CM to control spin angular momentum and whole-body angular excursions. For example, the moment about the CM has to be continually adjusted throughout a walking gait cycle to keep spin angular momentum and whole-body angular excursions from becoming appreciably large. To address spin angular momentum and the moment about the CM in connection with various postural balance strategies, the CMP ground reference point was recently introduced (Herr, Hofmann, and Popovic 2003; Hofmann 2003; Popovic, Hofmann, and Herr 2004a). Goswami and Kallem (2004) proposed the same point in an independent investigation.[4]

3.3.2. Definition

The CMP is defined as the point where a line parallel to the ground reaction force, passing through the CM, intersects with the external contact surface (see Figure 4). This condition can be expressed mathematically by requiring that the cross product of the CMP–CM position vector and the ground reaction force vector vanishes, or

$$(\vec{r}_{CMP} - \vec{r}_{CM}) \times \vec{F}_{G.R.} = 0 \text{ and } z_{CMP} = 0. \qquad (18)$$

By expanding the cross product of eq. (18), the CMP location can be written in terms of the CM location and the ground reaction force, or

$$x_{CMP} = x_{CM} - \frac{F_{G.R.X}}{F_{G.R.Z}} z_{CM} \qquad (19)$$

and

$$y_{CMP} = y_{CM} - \frac{F_{G.R.Y}}{F_{G.R.Z}} z_{CM}.$$

Finally, by combining ZMP eq. (6) and CMP eq. (19), the CMP location may also be expressed in terms of the ZMP location, the vertical ground reaction force, and the moment about the CM, or

$$x_{CMP} = x_{ZMP} + \frac{\tau_y(\vec{r}_{CM})}{F_{G.R.Z}} \qquad (20)$$

and

$$y_{CMP} = y_{ZMP} - \frac{\tau_x(\vec{r}_{CM})}{F_{G.R.Z}}.$$

4. Popovic, Hofmann, and Herr (2004a) called the specified quantity the zero spin center of pressure (ZSCP) point, whereas Goswami and Kallem (2004) called the specified quantity the zero rate of angular momentum (ZRAM) point. In this paper, we use a more succinct name, the centroidal moment pivot (CMP).

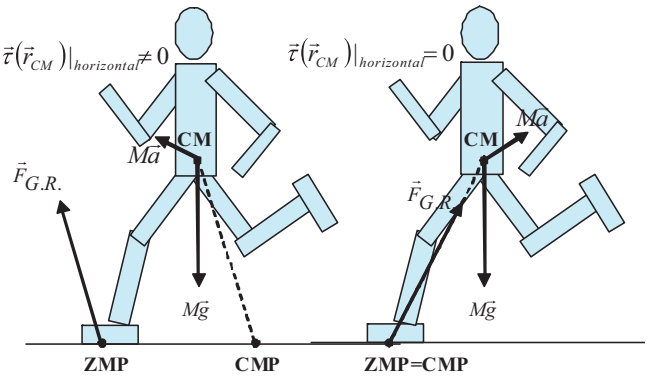

Fig. 4. Centroidal moment pivot. The CMP is the point where the ground reaction force would have to act to keep the horizontal component of the whole-body angular momentum constant. When the moment about the CM is zero (shown in the figure to the right), the CMP coincides with the ZMP. However, when the CM moment is non-zero (figure on the left), the extent of separation between the CMP and ZMP is equal to the magnitude of the horizontal component of moment about the CM, divided by the normal component of the ground reaction force.

As shown by eq. (20), when the CMP is equal to the ZMP, the ground reaction force passes directly through the CM of the body, satisfying a zero moment or rotational equilibrium condition. In distinction, when the CMP departs from the ZMP, there exists a non-zero body moment about the CM, causing variations in whole-body, spin angular momentum. While by definition the ZMP cannot leave the ground support base, the CMP can, but only in the presence of a significant moment about the CM. Hence, the notion of the CMP, applicable for both single and multileg ground support phases, is that it communicates information about whole-body rotational dynamics when supplemented with the ZMP location (excluding body rotations about the vertical axis).

It is interesting to note that when the stance foot is at rest during single support, and when there is zero moment about the CM, the ZMP, FRI, and CMP coincide. However, generally speaking, these ground reference points cannot be considered equivalent.

4. ZMP, FRI, and CMP Trajectories in Human Walking

For the diversity of biological motor tasks to be represented in a robot's movement capabilities, biomechanical movement strategies must first be identified, and legged control systems must exploit these strategies. To this end, we ask what are the characteristics of the ZMP, FRI, and CMP ground reference points in human walking, and how do they interrelate?

As discussed in Section 3, the separation distance between the FRI point and the ZMP should, in principle, be a reasonable indicator of foot rolling or angular acceleration. Hence, we anticipate that the FRI trajectory will closely track the ZMP trajectory throughout the controlled dorsiflexion phase of single support, when the foot is predominantly flat on the ground. However, during the powered plantar flexion phase, as the foot rolls and experiences acceleration, we expect the FRI point to diverge significantly from the ZMP trajectory, leaving the ground support base. In addition to the FRI reference trajectory, we also study the character of the CMP trajectory in human walking. As discussed in Section 3, spin angular momentum remains small throughout the walking cycle. Hence, we hypothesize that the CMP trajectory will never leave the ground support base during the entire walking gait cycle, closely tracking the ZMP trajectory during both single and double support phases.

In this section we test both the FRI and CMP hypotheses using a morphologically realistic human model and kinetic and kinematic gait data measured from ten human subjects walking at self-selected forward walking speeds. In Section 4.1, we outline the experimental methods used in the study, including a description of data collection methods, human model structure and the analysis procedures used to estimate, compare and characterize the reference point biological trajectories. Finally, in Section 4.2, we present the experimental results of the gait study, and in Section 4.3, we discuss their significance.

4.1. Experimental Methods

4.1.1. Kinetic and Kinematic Gait Measures

For the human walking trials, kinetic and kinematic data were collected in the Gait Laboratory of Spaulding Rehabilitation Hospital, Harvard Medical School, Boston, MA, in a study approved by the Spaulding Committee on the Use of Humans as Experimental Subjects. Ten healthy adult participants, five male and five female, with an age range from 20 to 38 years old, were involved in the study.

Participants walked at a self-selected forward speed over a 10 m long walkway. To ensure a consistent walking speed between experimental trials, participants were timed across the 10 m walking distance. Walking trials with forward walking speeds within a $\pm 5\%$ interval were accepted. Seven walking trials were collected for each participant.

To assess gait kinematics, an eight infrared camera, motion analysis system (VICON 512 System, Oxford Metrics, Oxford, UK) was used to measure the three-dimensional positions of reflective markers placed on various parts of each participant's body. The frame rate of the camera system was 120 frames per second. A total of 33 markers were employed: 16 lower extremity markers, five thoracic and pelvic markers, eight upper extremity markers, and four head markers. The markers were attached to the following bony landmarks: bilateral anterior superior iliac spines, posterior superior iliac spines, lateral femoral condyles, lateral malleoli, forefeet and heels. Additional markers were rigidly attached to wands over the mid-femur and mid-shaft of the tibia. Kinematic data of the upper body were also collected with markers placed on the following locations: sternum, clavicle, C7 vertebra, T10 vertebra, head, and bilaterally on the shoulder, elbow and wrist. Depending on the position and movement of a participant, the system was able to detect marker position with a precision of a few millimeters.

During walking trials, ground reaction forces were measured synchronously with the kinematic data using two staggered force platforms (model OR6-5-1, AMTI, Newton, MA) embedded in the 10 m walkway. The force data were collected at a sampling rate of 1080 Hz at an absolute precision of $\sim$0.1 N for ground reaction forces and $\sim$1 mm for the ZMP location.

4.1.2. Human Model Structure

A morphologically realistic human model was constructed in order to calculate the FRI and CMP ground reference trajectories. The human model, shown in Figure 5, consisted of 18 links: right and left forefoot links, heels, shanks, thighs, hands, forearms, upper arms, pelvis–abdomen region, thorax, neck, and head. The forefoot and a heel sections, as well as the hands, were modeled as rectangular boxes. The shanks, thighs, forearms, and upper arms were modeled as truncated cones. The pelvis–abdomen region and the thoracic link were modeled as elliptical slabs. The neck was modeled as a cylinder, and the head was modeled as a sphere.

To increase the accuracy of the human model, 25 length measurements were taken on each participant: (1) foot and hand length, width, and thickness; (2) shanks, thighs, forearms, and upper arm lengths as well as their proximal and distal base radii; (3) thorax and pelvis–abdomen heights, widths, and thicknesses; (4) radius of the head. The neck radius was set equal to half the head radius.

Using observations of the human foot's articulated bone structure (Ankrah and Mills 2003), the mass of the forefoot was estimated to be 20% of the total foot mass. For the remaining model segments, a link's mass and density were optimized to closely match experimental values in the literature (Winter 1990; Tilley and Dreyfuss 1993) using the following procedure. The relative mass distribution throughout the model, described by a 16-component vector D (i.e., the heel and forefoot were represented as a single foot segment) was modeled as a function of a single parameter α such that

$$D(\alpha) = (D_A + \alpha D_S)\big/(1 + \alpha). \tag{21}$$

Here, D_A is the average relative mass distribution obtained from the literature (Winter 1990), and the subject specific relative mass distribution, D_S, was obtained by using an equal density assumption; the relative mass of the ith link, D_S^i,was

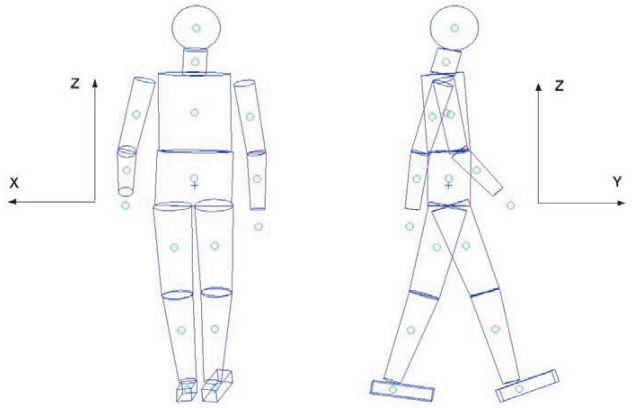

Fig. 5. The morphologically realistic human model used in the human gait study. The human model has a total of 38 degrees of freedom, or 32 internal degrees of freedom (12 for the legs, 14 for the arms and six for the rest) and six external degrees of freedom (three body translations and three rotations). Using morphological data from the literature and direct human participant measurements, mass is distributed throughout the model's links in a realistic manner.

assumed to be equal to the ratio of the link's volume, V^i, over the total body volume, V, or $D_S^i = V^i / V$. The selection of parameter α then uniquely defined the density profile throughout the various links of the human model, as described by the 16-component vector $P(\alpha)$, such that $P^i(\alpha) = M\, D^i(\alpha) / V^i$ where M was equal to the total body mass. The resulting relative mass distribution, D_R, was obtained as $D_R = D(\alpha_{min})$ where α_{min} minimized the absolute error between the distribution of link densities, $P(\alpha)$, and the average distribution of link densities obtained from the literature, P_A (Winter 1990). In notation form, this analysis procedure may be expressed as

$$\min\ |P(\alpha) - P_A| = \min \sqrt{\sum_i \left[P^i(\alpha) - P_A^i\right]^2} \Rightarrow \alpha_{min}$$

$$\Rightarrow D_R = \frac{D_A + \alpha_{min}\, D_S}{1 + \alpha_{min}}. \tag{22}$$

4.1.3. Data Analysis

For each participant and for each walking trial, the ZMP, FRI and CMP trajectories were computed. The ZMP was estimated directly from the force platform data using eq. (1). The FRI point was calculated based on eq. (10) using ground reaction force and foot kinematic gait data. The CMP was calculated using the calculated CM position from the human model, and the measured ZMP and ground reaction force data from the force platforms (see eq. 19). Here the CM trajectory was estimated by computing the CM of the human model at each gait posture throughout the entire gait cycle. The model's posture, or spatial orientation, was determined from the joint position data collected from the human gait trials.

As a measure of how well the FRI tracked the ZMP, and how well the CMP tracked the ZMP, we computed the linear distance between the FRI and the ZMP, as well as between the CMP and the ZMP, at each moment throughout the gait cycle. For each participant, the mean FRI–ZMP distance and the mean CMP–ZMP distance were then computed using all seven gait trials. These mean distances were then normalized by the participant's foot length. We then performed a non-parametric Wilcoxon signed rank test for zero median to test for significance in the mean FRI–ZMP normalized distance between the single support period of controlled dorsiflexion and the single support period of powered plantar flexion (N = 10 subjects). Finally, we again performed a non-parametric Wilcoxon signed rank test for zero median to test for significance in the mean CMP–ZMP distance between the single and double support phases of gait (N = 10 subjects). For these statistical analyses, significance was determined using $p < 0.05$.

4.2. Results

Representative trajectories of the ZMP, FRI, and CMP are shown in Figure 6 for a healthy female participant (age 21, mass 50.1 kg, height 158 cm, speed $\sim$1.3 m s^{-1}). For each study participant, Table 1 lists the mean normalized distances between the FRI and the ZMP, and additionally between the CMP and the ZMP.

For all participants and for all walking trials, the ZMP was always well inside the ground support base. The ZMP was never closer to the edge of the ground support base than by approximately 5–10% of foot length (see Figure 6). Additionally, for all participants and for all walking trials, the FRI point remained within the ground support base throughout the entire single support phase, even during powered plantar flexion, or heel-off, when the foot experienced acceleration. The mean of the normalized distance between the FRI and the ZMP for the controlled dorsiflexion phase ($0.04 \pm 0.01\%$) was significantly different from that computed for the powered plantar flexion phase ($0.19 \pm 0.06\%$) ($p = 0.002$). Finally, for all participants and for all walking trials, the CMP remained within ground support base throughout the entire gait cycle. The mean of the normalized distance between the CMP and the ZMP for the single support phase ($14 \pm 2\%$) was not significantly different from that computed for the double support phase ($13 \pm 2\%$) ($p = 0.35$).

4.3. Discussion

4.3.1. Human Walking Trajectories: FRI and ZMP

In this paper, we study the characteristics of the FRI ground reference point in human walking, and how it relates to the foot–ground ZMP. Since the FRI was proposed as an indicator of foot rotation (Goswami 1999), we hypothesize that

Table 1.

Subjects	1	2	3	4	5	6	7	8	9	10	Mean ±STD
A%	16	14	13	17	16	10	12	11	15	15	14 ± 2
B%	15	13	10	15	12	9.0	14	15	15	14	13 ± 2
C%	16	13	12	16	15	10	12	12	15	15	14 ± 2
D%	0.03	0.03	0.02	0.05	0.06	0.03	0.02	0.03	0.04	0.05	0.04 ± 0.01
E%	0.15	0.15	0.11	0.23	0.30	0.15	0.11	0.20	0.23	0.24	0.19 ± 0.06
F%	0.05	0.06	0.04	0.09	0.11	0.05	0.04	0.06	0.07	0.09	0.07 ± 0.02

For ten healthy test participants walking steadily at their self-selected speeds, we list the mean distances, normalized by foot length, between the CMP and the ZMP points for the single-support phase (A), double-support phase (B), and across the entire gait cycle (C). In addition, the table lists the mean distances, normalized by foot length, between the FRI and the ZMP points for controlled dorsiflexion (D), powered plantar flexion (E), and the entire single support phase (F).

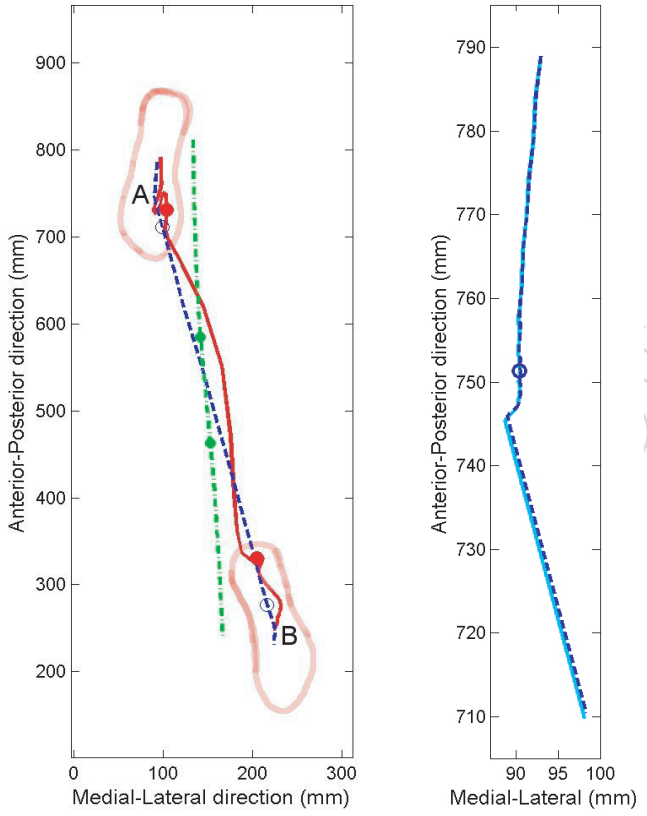

Fig. 6. Plotted on the left are the ZMP (dashed), CMP (solid), and CM ground projection (dash-dotted) trajectories and corresponding footprints of a study participant walking at a self-selected speed ($1.3\ \mathrm{m\,s^{-1}}$). The two circles on each line denote the transition from single to double support, and vice versa. Data span from the middle of a single support phase to the middle of the next single support phase of the opposite limb. Plotted on the right are the ZMP (dashed) and FRI (solid) trajectories from mid-stance to the double-support phase. Here the circle denotes the transition from foot-flat to heel-off.

the FRI will closely track the ZMP in early single support when the foot remains flat on the ground, but will then significantly diverge from the ZMP in late single support, leaving the ground support base as the foot undergoes acceleration during heel-off. The results of this investigation, however, do not support this hypothesis. We find that the FRI never leaves the ground support base, and that the mean FRI–ZMP separation distance during the single support phase is small (0.1% of foot length). The FRI point closely tracks the ZMP throughout the entire single support phase, with a mean FRI–ZMP separation equal to less than 1 mm. Clearly, during the foot-flat phase, one would not expect a large separation distance between the FRI and ZMP points because the stance foot does not rotate. However, during the heel-off or powered plantar flexion phase, encompassing on average 20% of the entire single support period (Wright, Desai and Henderson 1964; Rose and Gamble 1994), the foot rolls and undergoes acceleration, and one would therefore expect a more significant FRI–ZMP separation.

The rather small size of the FRI–ZMP separation in human walking, even when the foot is rolling, is perhaps due to the fact that the foot is small compared to the rest of body (foot mass is ∼1/70 of total body mass), and the corresponding rotational dynamics are therefore dictated by relatively small moments. From eq. (8), the FRI–ZMP separation is proportional to the foot's rate of change of angular momentum. This, in turn, depends on the foot's rotational acceleration and its moment of inertia. Compared to the entire body, the foot has a relatively small mass, and therefore, unless the foot has a very large angular acceleration, its rate of angular momentum change is relatively small compared to the entire body.

One might be inclined to expect that a more rigid and somewhat heavier robotic foot would result in a more pronounced FRI–ZMP separation. However, such a foot would likely result in a maximum FRI–ZMP separation of only a few millimeters. Consider the situation where a foot, $m_{foot} \approx M/70$, starting from rest, rotates through an angle, $\theta = \pi/6$, with constant angular acceleration during time interval, $\Delta t =$

0.1 s. Assuming that the foot may be approximated by a uniform rod of length $l_{foot} \approx 0.25$ m and that the vertical ground reaction force is approximately equal to body weight, one could solve eq. (8) for a typical FRI–ZMP separation at the moment of heel-off, or

$$|y_{FRI} - y_{CP}| = \frac{\frac{1}{3} m_{foot} l_{foot}^2 \left[2\theta/(\Delta t)^2\right]}{Mg - m_{foot} \frac{l_{foot}}{2} \left[2\theta/(\Delta t)^2\right]} = \frac{\frac{1}{3} 0.25^2 \left[2\frac{\pi}{6}/(0.1)^2\right]}{70 \cdot 9.81 - \frac{0.25}{2} \left[2\frac{\pi}{6}/(0.1)^2\right]} \approx 3.2\,\text{mm}. \tag{23}$$

Therefore, even for this exaggerated physical situation, we still obtain a FRI–ZMP separation of only a few millimeters. This obviously represents an obstacle for the FRI point as an indicator of foot acceleration in legged systems because both the ZMP and support base parameters are usually only known up to a few millimeters of accuracy. As a possible resolution to this difficulty, we propose a modified FRI point in Section 5.2.

4.3.2. Human Walking Trajectories: ZMP and CMP

Since spin angular momentum has been shown to remain small throughout the walking cycle, we hypothesize that the CMP will never leave the ground support base throughout the entire gait cycle, closely tracking the ZMP. The results of this investigation support this hypothesis. We find that the CMP never leaves the ground support base, and the mean separation distance between the CMP and ZMP is small (14% of foot length), highlighting how closely the human body regulates spin angular momentum in level ground walking. The mean normalized distance between the CMP and the ZMP for the single support phase ($14 \pm 2\%$) was not significantly different from that computed for the double support phase ($13 \pm 2\%$) ($p = 0.35$), suggesting that the CMP is a reasonable estimate of ZMP position independent of the number of legs in contact with the ground surface.

5. Control Implications of Ground Reference Points ZMP, FRI, and CMP

In this section, we discuss how the ZMP, FRI, and CMP ground reference points can be used in legged robotic and prosthetic control systems. In Section 5.1, the control implications of the foot–ground ZMP are discussed. In Section 5.2, we address the relatively small separation distance between the FRI and ZMP points and suggest a modified FRI that has a better scaling property. Finally, in Section 5.3, we discuss how the control of both the ZMP and the CMP could enhance postural stability for single-leg standing.

5.1. Control Implications of the ZMP

5.1.1. Does a ZMP Location Inside the Ground Support Base Indicate Postural Stability?

As noted by Goswami (1999), the requirement that the ZMP should be inside the ground support base has been extensively used in the literature as a criterion of postural stability[5] (Shih et al. 1990; Li, Takanishi and Kato 1993; Shih 1996; Arakawa and Fukuda 1997; Huang et al. 2001). However, since the ZMP must always reside within the ground support base as required by fundamental physics (see eq. 1), a ZMP estimate that falls outside the ground support base should be an indication of non-physical behavior and not an indication of overall postural instability. For example, if a computer simulation predicts that the ZMP is outside the ground support base, the result should simply be viewed as a non-physical simulation artifact and not an indication of postural instability. Still further, if the simulation predicts a ZMP location within the ground support base, overall postural stability is not, in any way, guaranteed.

5.1.2. Does Maintaining the ZMP at the Center of the Ground Support Envelope Guarantee Postural Stability?

It has been suggested in the literature that postural stability during single support will be ensured if the ZMP remains at the center of the ground support envelope (Vukobratovic and Juricic 1969; Vukobratovic and Stepanenko 1973; Li, Takanishi and Kato 1993; Arakawa and Fukuda 1997; Huang et al. 2001). However, it is noted here that accurately controlling the ZMP location to coincide with the center of the ground support envelope will not in itself guarantee postural stability for all legged control problems. To clarify this point, consider the simple model of single support standing shown in Figure 7(A). The mass of the body is represented as a point mass attached to a massless foot and leg linkage, and the ankle is the only actuated degree of freedom.

If the ZMP is tightly controlled to operate at the center of the ground support envelope, such that $x_{ZMP} = 0$, then according to eq. (6)

$$F_x = M\ddot{x}_{CM} = M\,(\ddot{z}_{CM} + g)\,\frac{x_{CM}}{z_{CM}} - \frac{\tau_y}{z_{CM}}. \tag{24}$$

For this simplified model, the moment about the CM is always equal to zero, $\tau_y = 0$, since the mass of the body is represented as a single point mass. Thus, from eq. (24) we have

$$\ddot{x}_{CM} = (\ddot{z}_{CM} + g)\,\frac{x_{CM}}{z_{CM}}. \tag{25}$$

We see from eq. (25) that for this simplified model, a control system that maintains the ZMP position at the center of the

5. Throughout this paper, postural stability, or body stability, refers to the maintenance of body attitude angles within a specified bounded region and the return to that bounded region after a perturbation (Vukobratovic, Frank, and Juricic 1970).

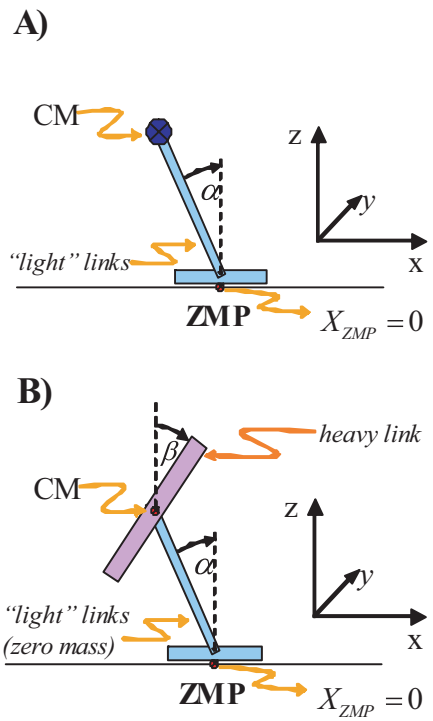

Fig. 7. In (A), a simple model of single-leg standing is shown consisting of three links: (1) a body link represented by a point mass equal to total body mass; (2) a massless leg link representing the stance leg; (3) a massless foot link (base of support), which is aligned with the ground and which has limited extent. The ankle joint between the foot link and the leg link is the only actuated degree of freedom in the model. In (B), the same model as in (A) is shown except the body link is modeled as a solid uniform rod. In contrast to the model of (A), the model of (B) has an actuated ankle and hip joint. Thus, this model may have a non-zero moment about its CM.

ground support envelope, or $x_{ZMP} = 0$, causes the system to be equivalent to a statically unstable, non-actuated inverted pendulum. Thus, we may conclude that controlling the ZMP to operate at the center of the ground support envelope during single support cannot, by itself, ensure postural stability.

If we now allow for non-zero ZMP positions, we obtain

$$\ddot{x}_{CM} = (\ddot{z}_{CM} + g)\frac{x_{CM} - x_{ZMP}}{z_{CM}}. \qquad (26)$$

Thus, we see from eq. (26) that by selecting an appropriate non-zero ZMP trajectory, the model of Figure 7(A) can be stabilized albeit for relatively modest CM disturbances.[6] For example, if the CM projection onto the ground extends beyond the boundaries of the foot as a result of a disturbance to the system, the system cannot be stabilized simply by controlling ZMP position because the foot is not physically attached to the ground surface (see eq. 26; Popovic and Herr 2003; Hofmann et al. 2004, Popovic, Hofmann and Herr 2004b).

Although controlling the ZMP position is one strategy for stabilizing legged posture, it is not the only tool for addressing stability. For example, during single-leg standing, consider shrinking the stance foot to a single point. The ZMP is then constrained at that contact point and cannot be repositioned using a ZMP control strategy. As is apparent from eq. (24), the only way to stabilize such a system is to produce a non-zero moment about the CM. In Section 5.3, we argue that by controlling both the ZMP and CMP ground reference positions, overall postural stability during single support standing can be maintained even in the presence of large disturbances where the CM projection on the ground surface extends beyond the ground support envelope.

5.2. Control Implications of the FRI

5.2.1. Can the FRI Point be Modified to Increase its Sensitivity to Non-Zero Foot Accelerations?

Gaswami (1999) introduced the FRI as a measure of foot rotational acceleration. He argued that the distance between the FRI point and the ZMP is useful because it communicates information about foot rotational dynamics during the single support phase (excluding foot rotations about the vertical axis). However, in this investigation we find that during the single support phase of walking, the FRI closely tracks the ZMP even though the foot is rolling and undergoing acceleration. During the entire single support phase, the absolute separation distance between the FRI and the ZMP is less than 1 mm. Clearly, during the foot-flat phase one should not expect a large separation between the FRI and ZMP because the stance foot does not rotate. However, during the heel-off or powered plantar flexion phase, the foot rolls and undergoes acceleration, and one would therefore expect a more significant FRI–ZMP separation.

One approach to resolve this problem is to use a modified FRI point (MFRI) defined as

$$(\vec{r}_{MFRI} - \vec{r}_{ZMP}) \times (m_{foot}\vec{g})|_{horizontal} = \left[\frac{d\vec{L}^{foot}(\vec{r}_{MFRI})}{dt}\right]_{horizontal}, \qquad (27)$$

where the moment due to the weight of the foot is employed instead of the moment due to the ground reaction force (see eq. 8 for the definition of the FRI). The MFRI–ZMP separation scales much better than the FRI–ZMP separation simply because $F_{G.R.Z} >> m_{foot}g$.

6. Here stability refers to the capacity of the system to restore the CM to a location vertically above the center of the ground support envelope ($x_{ZMP} = 0$) after a perturbation.

Although the MFRI point described in eq. (27) cannot be represented by body–foot dynamics alone (see eq. 15), the point may be used to quantify non-zero foot moments and therefore stance foot rotational instabilities. To highlight the differences between the original FRI and the MFRI in terms of their capacity to detect foot rotational accelerations, we construct a simple model of the foot. Assuming that the foot may be approximated by a uniform rod rotating about its "toes" and that the vertical ground reaction force is equal to body weight, eq. (8) can be solved for a typical FRI–ZMP separation as function of the relative heel acceleration, $x = {}^{2a_{foot}}/_{g}$, at the moment of heel-off, or

$$\frac{|y_{FRI} - y_{ZMP}|}{l_{foot}} = \frac{x/3}{(M/m_{foot}) - (x/2)} \text{ for } x < \frac{2M}{m_{foot}}. \quad (28)$$

Under the aforementioned approximations, one could also solve for a typical MFRI–ZMP separation distance, or

$$\frac{|y_{MFRI} - y_{ZMP}|}{l_{foot}} = \frac{x/3}{1 - (x/2)} \text{ for } x < 2. \quad (29)$$

The original FRI and the MFRI separation distances from the ZMP point are shown in Figure 8(A) assuming $m_{foot} \approx M/70$. From the human walking data, a typical peak foot acceleration during the powered plantar flexion phase of single support is $x_{peak} = {}^{2a_{foot}}/_{g} \sim 1$. At this peak value, the MFRI–ZMP separation distance is ∼20cm whereas the FRI–ZMP separation is only ∼1 mm. In Figure 8(B), the original FRI, the modified FRI, and the ZMP are plotted for the single support phase of human walking, clearly indicating that the MFRI–ZMP separation distance is sufficiently large to be a measurable physical quantity given the resolution of current sensing technology.

5.2.2. Can the Modified FRI Point be Employed as a Measure of Postural Stability?

Although stance-foot rotational acceleration may be an important indicator of a loss of overall postural balance for some legged movement activities, a lack of foot rotational equilibrium is clearly not always related to overall postural instability. For example, it is easy to imagine situations where the stance foot is rolling but postural stability of a legged system is perfectly satisfied. In fact, during a large portion of the human gait cycle, the stance foot is not in perfect rotational equilibrium even during the single support phase (Rose and Gamble 1994). Although postural stability and stance foot equilibrium are not always inter-related, rotational equilibrium of the foot is indeed one measure that might be useful in the evaluation and control of legged systems (Hofmann et al. 2004).

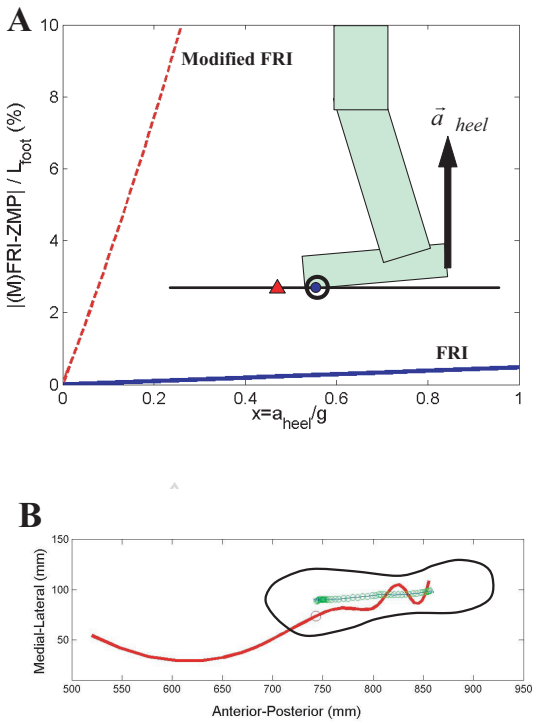

Fig. 8. In (A), predictions from the simplified foot model are shown. The FRI–ZMP separation and the modified FRI–ZMP separation, each normalized by foot length, are plotted as a function of heel acceleration normalized by gravitational acceleration. As shown, this calculation assumes a flat contact surface, a rectangular foot shape, and a foot CM position at ground level when the heel first lifts from the ground surface. In the foot illustration, the open circle is the ZMP, the closed circle is the original FRI, and the closed triangle is the modified FRI. In (B), the ZMP (dashed line), the original FRI (open circles), and the modified FRI (solid line) are plotted for the single support phase of human walking. Although the results are from a single study participant (female, mass = 50.1 kg) walking at a self-selected speed, similar results were observed for all participants and for all walking trials. The large circle on the modified FRI (solid line) denotes the transition from the foot-flat phase of single support to the introduction of heel-off and powered plantar flexion. The modified FRI remains close to the ZMP during the foot-flat phase but then diverges from the ZMP as the foot experiences rotational accelerations during powered plantar flexion.

5.3. Control Implications of the CMP

5.3.1. For Whole-body Rotational Control, Should a Control System Minimize CM Moment, Spin Angular Momentum, or Whole-Body Angular Excursions?

As noted in Section 4.2, the CMP trajectory was confined to the ground support base for each subject and for each

walking trial. Thus, one metric of human-like walking that may be useful in the evaluation of biomimetic humanoid robots is that the CMP must remain within the ground support base, near the ZMP, throughout the entire gait cycle. However, a zero moment about the CM, or a zero CMP–ZMP separation, should only be viewed as a condition of body rotational equilibrium and not a condition of postural stability. A loss of rotational equilibrium does not necessarily mean that the person or robot is destined to fall. In fact, the moment about the CM is prominently non-zero for many stable legged movement patterns (Hinrichs, Cavanagh and Williams 1983; Dapena and McDonald 1989; LeBlanc and Dapena 1996; Gu 2003). Non-zero CM moments are expected since the application of CM moment by a legged control system can increase the restoring force applied to the CM, as shown by eq. (6), restoring CM position to a desired location (Hofmann et al. 2004;Popovic, Hofmann, and Herr 2004a,b).

Since the application of moments about the CM is one critical control strategy to achieve postural stability in the presence of disturbances, the objective for the controller of whole-body angular behavior should not be to achieve a zero CM moment, or equivalently, a zero CMP–ZMP separation. Rather, a CM moment should be applied by the system controller to achieve a desired spin angular momentum and a particular whole-body angular excursion (see eq. 17). For example, focusing solely on rotational degrees of freedom, one could write a simple second-order differential control equation for a desired target moment, or

$$\begin{aligned}\vec{\tau}_{des.}(\vec{r}_{CM}) &= \dot{\vec{L}}_{des.} + \overleftrightarrow{a}\,\Delta\vec{\theta} + \overleftrightarrow{b}\,\Delta\dot{\vec{\theta}} \\ &= \dot{\vec{L}}_{des.} + \overleftrightarrow{a}\,\Delta\vec{\theta} + \overleftrightarrow{b}'\,\Delta\vec{L}(\vec{r}_{CM}), \qquad (30)\end{aligned}$$

where $\Delta\vec{L}(\vec{r}_{CM}) = \vec{L}(\vec{r}_{CM}) - \vec{L}_{des.}(\vec{r}_{CM})$ and $\Delta\vec{\theta} = \vec{\theta} - \vec{\theta}_{des.}$, $\overleftrightarrow{a}$ and $\overleftrightarrow{b}$ (with $\overleftrightarrow{b}' = \overleftrightarrow{b}\,\overleftrightarrow{I}^{-1}(\vec{r}_{CM})$) are second-order tensors, i.e., 3×3 matrices representing rotational "stiffness" and "damping" coefficients, respectively, $\overleftrightarrow{I}(\vec{r}_{CM}) = \sum_{i=1}^{N} \overleftrightarrow{I}_i(\vec{r}_{CM})$ is the whole-body moment of inertia tensor about the CM (also a function of time) and $\vec{\omega} = \overleftrightarrow{I}^{-1}(\vec{r}_{CM})\,\vec{L}(\vec{r}_{CM})$ is the whole-body effective angular velocity (which may be integrated to give $\vec{\theta}$), see eq. (17). Alternatively, instead of whole-body angular excursions, which are not directly measurable quantities, one may consider using whole-body principal angles defined by the relative orientations of the principal axes of the whole-body moment of inertia tensor with respect to the non-rotating lab frame axes (Popovic and Herr 2005). For a humanoid walking robot, the desired whole-body angular excursion and the spin angular momentum would both be set to zero and the rotational stiffness and damping coefficients would then be adjusted to achieve a desired system response.

In his book *Legged Robots that Balance*, Raibert (1986) speculated that a control system that keeps angular momentum constant during stance could achieve higher efficiency and better performance. Motivated by biomechanical measurements showing the relatively small size of CM moments during human walking, Popovic, Gu and Herr (2002) suggested that humanoid control systems should explicitly minimize global spin angular momentum during steady state forward walking ($\vec{L}_{des.}(\vec{r}_{CM}) = 0$). Using this approach, the zero-spin controller would apply corrective moments to minimize body spin when the whole-body state is such that spin is non-zero. It is noted here that a consequence of this control objective is that the CMP–ZMP separation distance is minimized. However, a control system that only minimizes the CMP–ZMP separation distance will only ensure a constant spin angular momentum and not specifically a zero spin value.

Kajita et al. (2003, 2004) implemented a zero-spin control on the humanoid robot HRP-2 and showed its usefulness in kicking, hopping and running. Still further, Popovic, Hofmann and Herr (2004a) showed in a two-dimensional numerical simulation of walking that biologically realistic leg joint kinematics emerge through the minimization of spin angular momentum and the total sum of joint torque squared (minimal effort criteria), suggesting that both angular momentum and energetic factors may be important considerations for biomimetic controllers.

5.3.2. Would Controlling Both ZMP and CMP Enhance Postural Stability?

For the simplified model of single-leg standing shown in Figure 7(A), Section 5.1, ankle torques have to be applied to move the ZMP such that appropriately needed horizontal forces are generated, as dictated by eq. (26), to move the model's CM back over the foot support envelope. However, as required by physics (see eq. 1), the ZMP cannot leave the ground support base. This physical constraint poses a restriction on the magnitude of the restoring CM forces that can be applied by the system controller to restore CM position, and therefore directly limits the range of perturbation that can be rejected by the system.

Let us now relax the zero moment condition (CMP=ZMP) and consider the model shown in Figure 7(B). In this model, the point mass of model 7A is replaced with a uniform rod that rotates about a hip joint at the top of a massless leg and foot linkage. By controlling both the ZMP and CMP trajectories, a larger set of perturbations can be rejected than when controlling only the ZMP trajectory (Hofmann et al. 2004; Popovic, Hofmann and Herr 2004a,b). Even when the ZMP is at the very edge of the ground support envelope in the model of Figure 7(B), a horizontal restoring force can still be produced through the application of a moment about the CM, or equivalently by controlling the CMP relative to the ZMP. According to eq. (6), the horizontal restoring force output of

the model shown in Figure 7(B) can now be written as

$$F_x = M\ddot{x}_{CM} = M\,(\ddot{z}_{CM} + g)\,\frac{x_{CM} - x_{ZMP}}{z_{CM}} - \frac{\tau_y}{z_{CM}}$$
$$= F_x^{zero-moment} + F_x^{moment} \tag{31}$$

where $F_x^{zero-moment} = M\,(\ddot{z}_{CM} + g)\,\frac{x_{CM} - x_{ZMP}}{z_{CM}}$ corresponds to a zero-moment balance strategy and $F_x^{moment} = -\frac{\tau_y}{z_{CM}}$ corresponds to a moment balance strategy. Because the CMP represents a unique pivot point, eq. (31) may be written more compactly as

$$F_x = M\,(\ddot{z}_{CM} + g)\,\frac{x_{CM} - x_{CMP}}{z_{CM}}. \tag{32}$$

As highlighted by eq. (32), the CM restoring force can be controlled by modulating the separation distance between the CM projection on the ground surface and the CMP location.

Depending on the character of a particular movement task and robotic structure, the two balance control strategies may have different levels of influence on postural stability. For example, in Figure 7(B), if the model's foot link were made infinitely small, with $x_{ZMP} = 0$ as a physical constraint, the moment balance strategy (CMP $\neq$ ZMP) would necessarily dominate. However, when the CMP is in the vicinity of the ground support envelope boundary during single-leg balancing, or outside that boundary, the moment balance strategy (CMP $\neq$ ZMP) must dominate since ZMP trajectory control alone cannot restore postural balance (Hofmann et al. 2004; Popovic, Hofmann and Herr 2004a,b). Therefore, the CMP location relative to the ground support envelope is an important indicator for a control system to determine which balance strategy should necessarily dominate (Hofmann et al. 2004; Popovic, Hofmann and Herr 2004a,b).

6. Summary

For the diversity of biological motor tasks to be represented in a robot's movement repertoire, biomechanical movement strategies must first be identified, and legged robotic control systems must exploit these strategies. To this end, in this paper we ask what are the characteristics of the ZMP, FRI, and CMP ground reference trajectories in human walking, and how do they inter-relate? We compute walking reference trajectories using a human model and gait data measured from ten human subjects walking at self-selected speeds. We find that the mean separation distance between the FRI and ZMP during the powered plantar flexion period of single support is within the accuracy of their measurement (0.1% of foot length), and thus the FRI point is determined not to be an adequate measure of foot rotational acceleration. As a potential resolution to this difficulty, we propose a modified FRI point with improved scaling properties. In addition, we find that the CMP never leaves the ground support base, and the mean separation distance between the CMP and the ZMP is small (14% of foot length) across both single and double support walking phases, highlighting how closely the human body regulates spin angular momentum in level ground walking.

We conclude the paper with a discussion of legged control issues related to the ground reference points. Using a simple model of single-leg balancing, we show that by controlling both the ZMP and the CMP trajectories, larger CM restoring forces can be applied by a system than would be possible using only a ZMP control. An area of future research of considerable importance will be in the implementation of legged systems that control both the ZMP and the CMP locations, resulting in corrective CM forces and moments necessary to restore CM position and body angular orientation. Another area of future research will be to characterize the ZMP and CMP biological trajectories for a whole host of animal and human movement patterns in the hope to further motivate biomimetic control schemes. It is our hope that this work will lead to further studies in ground reference points for the identification and control of legged systems, resulting in an even wider range of locomotory performance capabilities of legged robots and prostheses.

Appendix A: Center of Pressure and Zero Moment Point: Equivalence and Uniqueness

Although several authors (Goswami 1999; Sardain and Bessonet 2004) have speculated that the CP should be equivalent to the ZMP,[7] no formal proof has yet been advanced. In this appendix, we put forth a formal proof of their equivalence for horizontal ground surfaces, and then we show their uniqueness for more complex contact topologies.

A.1. Equivalence of the ZMP and the CP for Horizontal Contact Surfaces

The concept of CP most likely originated from the field of fluid dynamics. CP is utilized in aerodynamical calculations of aircraft and rockets (Darling 2002). It is also frequently used in the study of human gait and postural balance (Winter 1990; Rose and Gamble 1994).

For a body resting on a flat horizontal ground surface, the position of the CP, denoted by $\vec{r}_{CP}$, is defined as

$$\vec{r}_{CP} = \frac{\int_{gsb} \vec{r}\; p\;(\vec{r})\;\mathrm{d}a}{\int_{gsb} p\;(\vec{r})\;\mathrm{d}a} = \frac{\vec{\tau}_{G.R.}(0)|_{horizontal}}{F_{G.R.\,Z}} \times \frac{\vec{g}}{g}, \tag{A1}$$

where the integration is over the ground support base (gsb), da is an infinitesimal element of the support surface located at $\vec{r}$, $p\;(\vec{r})$ is the pressure at that location, $F_{G.R.\,Z}$ is the vertical component of the resulting ground reaction force, and g is the

7. Goswami (1999) and Sardain and Bessonet (2004) did not prove the equivalence of the CP and the ZMP, but rather, they proved the equivalence of two definitions of the ZMP (see Section 3.1 for ZMP definitions, eqs. 1 and 2).

gravitational acceleration. The second equality in equation (A1) follows from $p(\vec{r})\,\mathrm{d}a = \mathrm{d}F_{G.R.\,Z}$ and $\vec{r}\cdot\vec{g} = 0$.

The resulting moment exerted from the ground on the body about the origin of the lab reference frame (assumed here to be on the ground) is

$$\vec{\tau}_{G.R.}(0)|_{horizontal} = \int_{gsb} \left(\vec{r} \times \mathrm{d}\vec{F}_{G.R.}\right)|_{horizontal}$$

$$= -\int_{gsb} \left(\vec{r} \times \frac{\vec{g}}{g}\right) p(\vec{r})\,\mathrm{d}a = \frac{\vec{g}}{g} \times \int_{gsb} \vec{r}\, p(\vec{r})\,\mathrm{d}a. \quad \text{(A2)}$$

For simplicity we assume a horizontal ground surface in eqs. (A1) and (A2). However, the results may easily be generalized to include inclined surfaces as well if vector $-\vec{g}/g$ is exchanged for $\vec{n}_{\perp}$, the unit vector normal to the surface and pointing away from the ground. In addition, $F_{G.R.\,Z}$ has to be exchanged with $F_{G.R.\perp}$, the component of the ground reaction force normal to the surface, and $\vec{\tau}|_{horizontal}$ has to be exchanged for $\vec{\tau}|_{||}$ where $\vec{\tau}|_{||}\cdot\vec{n}_{\perp} = 0$. For a more complicated surface geometry, for example when two robot legs are posed on two surfaces of different inclination, the unique embedding surface does not exist. Below, we resolve this issue by considering an embedding convex volume instead of an embedding flat surface. The flat surface approach was first proposed by Takanishi et al. (1990) and later used by Sardain and Bessonnet (2004).

Given the definition of the CP (eq. A.1), we can prove that the CP is identical to the ZMP by noting from eq. (A2) that

$$\vec{\tau}_{G.R.}(\vec{r}_{CP})|_{horizontal} = \vec{\tau}_{G.R.}(0)|_{horizontal} + F_{G.R.\,Z}\vec{r}_{CP} \times \frac{\vec{g}}{g} = 0, \quad \text{(A3)}$$

therefore satisfying one definition of the ZMP defined in eq. (1), Section 3.1.

Alternatively we could rewrite eq. (1), Section 3.1, as

$$\vec{\tau}_{G.R.}(\vec{r}_{ZMP})|_{horizontal} = \int_{gsb} \left[(\vec{r} - \vec{r}_{ZMP}) \times \mathrm{d}\vec{F}_{G.R.}\right]_{horizontal}$$

$$= -\int_{gsb} \left[(\vec{r} - \vec{r}_{ZMP}) \times \frac{\vec{g}}{g}\right] \mathrm{d}F_{G.R.Z} = 0, \quad \text{(A4)}$$

to show that it is exactly satisfied when the ZMP is identical to the CP (eq. A.1), or

$$\vec{\tau}_{G.R.}(\vec{r}_{ZMP})|_{horizontal} = -\int_{gsb} \left(\vec{r} \times \frac{\vec{g}}{g}\right) \mathrm{d}F_{G.R.Z}$$

$$+ \frac{\int_{gsb} \vec{r}\,\mathrm{d}F_{G.R.Z}}{\int_{gsb} \mathrm{d}F_{G.R.Z}} \times \frac{\vec{g}}{g} \int_{gsb} \mathrm{d}F_{G.R.Z} = 0 \quad \text{QED.} \quad \text{(A5)}$$

Hence, for a flat horizontal support base, the ZMP and the CP exactly coincide.

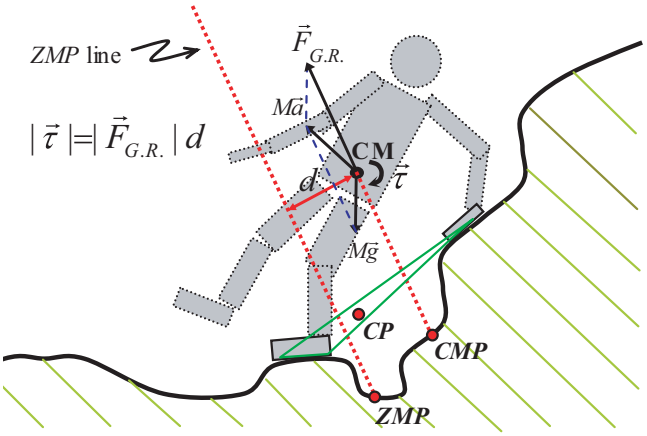

Fig. A1. Dynamical multilink humanoid model with hand and foot contact. The ground reaction force originates at the ZMP. Inertia and the force of gravity originate at the CM point. As shown in the figure, the ZMP and the CP point do not coincide for non-horizontal contact surfaces.

A.2. Uniqueness of the ZMP and the CP for Complex Contact Topologies

Consider the human model shown in Figure A1. Here the model's hand and foot are exerting forces against a non-horizontal contact surface. Given the net CM force, the ground reaction force may be obtained by simply subtracting the gravitational force. Given the CM location and the net moment about the CM, the ZMP line may be constructed. The intersection of that line with the contact surface then defines the ZMP location. In distinction, the CP may be obtained by integrating across the contact surface according to the first equality of eq. (A1). Hence, the CP can be positioned anywhere inside the convex hull represented by a three-dimensional, CP embedding volume and encompassing the contact foot and contact hand. For this particular example, the CP is not a ground reference point at all but is located above the contact surface.

Using mathematical notation, we show that the ZMP is not equal to the CP for non-horizontal contact surfaces like those depicted in Figure 8. For a general distribution of a normal unit vector field, $\vec{n}_{\perp}(\vec{r}) \neq \overrightarrow{\text{const.}}$, defined on all contact surfaces, one may show that the ZMP is not equal to the CP by first defining the ZMP as

$$\left[\int_{sb} (\vec{r} - \vec{r}_{CM}) \times \mathrm{d}\vec{F}_{R.}\right]_{hor.} = \left[(\vec{r}_{ZMP} - \vec{r}_{CM}) \times \int_{sb} \mathrm{d}\vec{F}_{R.}\right]_{hor.} \quad \text{(A6)}$$

where $\vec{r}_{ZMP}$ is on the external contact surface. We can then set this definition of the ZMP equal to the CP (eq. A.1), to

observe that

$$\int_{sb} \left(\vec{r} \times \mathrm{d}\vec{F}_R\right)_{hor.} \neq \left[\frac{\int_{sb} \vec{r}\left(\mathrm{d}\vec{F}_{R.} \cdot \vec{n}\right)}{\int_{sb}\left(\mathrm{d}\vec{F}_{R.} \cdot \vec{n}\right)} \times \int_{sb} \mathrm{d}\vec{F}_{R.}\right]_{hor.} . \quad \text{(A7)}$$

Hence, the ZMP and the CP do not always coincide and should therefore not be considered identical physical quantities. It should be noted that for expressions (A6) and (A7) we avoided the prefix "ground" to stress that any type of external contact surface is permissible when the ZMP is defined according to eq. (A6). Also, using this formalization, any body segment may be in contact with the external surface.

Acknowledgments

The authors wish to thank Paolo Bonato and Jennifer Lelas at the Spaulding Rehabilitation Hospital Gait Laboratory, Boston, MA, for their helpful suggestions and support. The authors also thank Waleed Farahat, Andreas Hofmann, Dan Paluska, Ben Swilling, and Russ Tedrake for their useful suggestions and technical support.

References

Ankrah, S. and Mills, N. J. 2003. Analysis of ankle protection in football. *Sports Engineering* 6.

Arakawa, T. and Fukuda, T. 1997. Natural motion generation of biped locomotion robot using hierarchical trajectory generation method consisting of GA, EP layers. *Proceedings of the IEEE International Conference on Robotics and Automation*, Albuquerque, NM, pp. 211–216.

Borelli, G. A. 1680. *De Motu Animalium* (English translation by P. Maquet, Springer-Verlag, Berlin, 1989).

Braune, W. and Fischer, O. 1895. Der Gang des Menschen. I Theil. *Abh. K. Sachs. Ges. Wiss. Math.-Phys. Classe*, 21:153.

Chew, C., Pratt, J., and Pratt, G. 1999. Blind walking of a planar bipedal robot on sloped terrains. *Proceedings of the IEEE International Conference on Robotics and Animation,* Detroit, MI.

Choi, J. H. and Grizzle, J. W. 2005. Planar bipedal walking with foot rotation. *American Control Conference (ACC).*

Dapena, J. and McDonald, C. 1989. A three-dimensional analysis of angular momentum in the hammer throw. *Med. Sci. in Sports Exercise* 21:206–220.

Darling, D. 2002. *The Complete Book of Spaceflight: From Apollo 1 to Zero Gravity,* Wiley, New York.

Dasgupta, A. and Nakamura, Y. 1999. Making feasible walking motion of humanoid robots from human motion capture data. *Proceedings of the IEEE International Conference on Robotics and Automation*, Detroit, MI, pp. 47–52.

Elftman, H. 1938. The measurement of the external force in walking. *Science* 88:152–153.

Elftman, H. 1939. The function of the arms in walking. *Human Biology* 11:529–535.

Elftman, H. and Manter, J. 1934. A cinematic study of the distribution of pressure in the human foot. *Science* 80:484.

Full, B. and Koditschek, D. 1999. Templates and anchors: neural mechanical hypotheses of legged locomotion on land. *Journal of Experimental Biology* 202:3325–3332.

Goswami, A. 1999. Postural stability of biped robots and the foot rotation indicator point. *International Journal of Robotics Research* 18(6):523–533.

Goswami, A. and Kallem, V. 2004. Rate of change of angular momentum and balance maintenance of biped robots. *Proceedings of the IEEE International Conference on Robotics and Automation*, New Orleans, LA, pp. 3785–3790.

Gu, W. 2003. The regulation of angular momentum during human walking, Undergraduate Thesis, Massachusetts Institute of Technology, Physics Department.

Herr, H. and Popovic, M. 2004. Angular momentum regulation in human walking. *Journal of Experimental Biology* in press.

Herr, H., Hofmann, A., and Popovic, M. 2003. New horizons for orthotic and prosthetic technology: merging body and machine. *Presented at the ZIF International Conference on Walking Machines*, Bielefeld, Germany.

Herr, H., Whiteley, G. P., and Childress, D. 2003. Cyborg Technology – Biomimetic Orthotic and Prosthetic Technology. *Biologically Inspired Intelligent Robots*, Y. Bar-Cohen and C. Breazeal, editors, SPIE Press, Bellingham, WA, pp. 103–143.

Hinrichs, R., Cavanagh, P., and Williams, K. 1983. Upper extremity contributions to angular momentum in running. *Biomechanics VIII-B,* Human Kinetics, Champaign, IL, pp. 641–647.

Hirai, K. 1997. Current and future prospective of Honda humanoid robot. *Proceedings of the IEEE/RSJ International Conference on Intelligent Robots and Systems,* Grenoble, France, pp. 500–508.

Hirai, K., Hirose, M., Haikawa Y., and Takenaka T. 1998. The development of Honda humanoid robot. *Proceedings of the IEEE International Conference on Robotics and Automation*, Leuven, Belgium, pp. 1321–1326.

Hofmann, A. 2003. Control rules for biomimetic human bipedal locomotion based on biomechanical principles. Ph.D. Thesis Proposal, submitted to the Computer Science and Electrical Engineering Department, Massachusetts Institute of Technology.

Hofmann, A., Popovic, M., Massaquoi, S., and Herr, H. 2004. A sliding controller for bipedal balancing using integrated

movement of contact and non-contact limbs. *Proceedings of the IEEE/RSJ International Conference on Intelligent Robots and Systems*, Sendai, Japan.

Huang, Q., Yokoi, K., Kajita, S., Kaneko, K., Aria, H., Koyachi, N., and Tanie, K. 2001. Planning walking patterns for a biped robot. *IEEE Transactions on Robotics and Automation* 17(3):280–289.

Kagami, S., Kanehiro, F., Tamiya, Y., Inaba, M., and Inoue, H. 2000. Autobalancer: an on-line dynamic balance compensation scheme for humanoid robots. *Proceedings of the 4th International Workshop on Algorithmic Foundations (WAFR '00)*, Hanover, NH, March 16–18, pp. SA-79–SA-89.

Kajita, S., Kanehiro, F., Kaneko, K., Fujiwara, K., Harada, K., Yokoi, K., and Hirukawa, H. 2003. Resolved momentum control: humanoid motion planning based on the linear and angular momentum. *Proceedings of the IEEE/RSJ International Conference on Intelligent Robots and Systems*, Las Vegas, NV, pp. 1644–1650.

Kajita, S., Nagasaki, T., Kaneko, K., Yokoi, K., and Tanie, K. 2004. A hop towards running humanoid biped. *Proceedings of the IEEE International Conference on Robotics and Automation*, New Orleans, LA, pp. 629–635.

Kondak, K. and Hommel, G. 2003. Control and online computation of stable movement for biped robots. *Proceedings of the International Conference on Intelligent Robots and Systems (IROS)*. Las Vegas, NV.

LeBlanc, M. and Dapena, J. 1996. Generation and transfer of angular momentum in the javelin throw. *Proceedings of the 20th Annual Meeting of the American Society of Biomechanics.* Atlanta, GA, pp.17–19.

Lee, W. and Raibert, M. 1991. Control of hoof rolling in an articulated leg. *Proceedings of the IEEE International Conference on Robotics and Automation*, Sacramento, CA, pp. 1386–1391.

Li, Q., Takanishi, A., and Kato, I. 1993. Learning control for a biped walking robot with a trunk. *Proceedings of the IEEE/RSJ International Conference on Intelligent Robots and Systems*, Yokohama, Japan, pp. 1771–1777.

Popovic, M. and Herr, H. 2003. Conservation of whole-body angular momentum. *Presented at the Neuro-Muscular Research Center Seminar Series*, Boston University, Boston, MA, March 20.

Popovic, M. and Herr, H. 2005. Global motion control and support base planning. *Proceedings of the IEEE/RSJ International Conference on Intelligent Robots and Systems*, Alberta, Canada.

Popovic, M., Gu, W., and Herr, H. 2002. Conservation of angular momentum in human movement. *MIT AI Laboratory – Research Abstracts, September 2002,* pp. 264–265.

Popovic, M., Englehart, A., and Herr, H. 2004. Angular momentum primitives for human walking: biomechanics and control. *Proceedings of the IEEE/RSJ International Conference on Intelligent Robots and Systems*, Sendai, Japan, pp. 1685–1691.

Popovic, M., Hofmann, A., and Herr, H. 2004a. Angular momentum regulation during human walking: biomechanics and control. *Proceedings of the IEEE International Conference on Robotics and Automation*, New Orleans, LA, pp. 2405–2411.

Popovic, M., Hofmann, A., and Herr, H. 2004b. Zero spin angular momentum control: definition and applicability. *Proceedings of the IEEE RAS/RSJ International Conference on Humanoid Robots*, Los Angeles, CA.

Pratt, G. 2002. Low impedance walking robots. *Integ. and Comp. Biol.* 42:174–181.

Raibert, M. 1986. *Legged Robots that Balance*, MIT Press, Cambridge, MA.

Rose, J. and Gamble, J. G. 1994. *Human Walking,* 2nd edition, Williams and Wilkins, Baltimore, MD.

Sardain, P. and Bessonnet, G. 2004. Forces acting on a biped robot. Center of pressure–zero moment point. *IEEE Transactions on Systems, Man and Cybernetics, Part A* 34(5):630–637.

Schaal, S. 1999. Is imitation learning the route to humanoid robots? *Trends in Cognitive Sciences* 3:233–242.

Shih, C. L. 1996. The dynamics and control of a biped walking robot with seven degrees of freedom. *ASME Journal of Dynamic Systems, Measurement and Control* 118:683–690.

Shih, C. L., Li, Y. Z., Churng, S., Lee, T. T., and Gruver W. A. 1990. Trajectory synthesis and physical admissibility for a biped robot during the single-support phase. *Proceedings of the IEEE/RSJ International Conference on Intelligent Robots and Systems*, pp. 1646–1652.

Takanishi, A., Ishida, M. Yamazaki, Y., and Kato, I. 1985. The realization of dynamic walking by the biped robot WL-10RD. *Proceedings of the International Conference on Advanced Robotics*, Tokyo, Japan, pp. 459–466.

Takanishi, A., Lim, H.-ok, Tsuda, M., and Kato, I. 1990. Realization of dynamic biped walking stabilized by trunk motion on a sagitally uneven surface. *Proceedings of the IEEE/RSJ International Conference on Intelligent Robots and Systems*, pp. 323–330.

Tilley A. R. and Dreyfuss H. 1993. *The Measure of Man and Woman*. Whitney Library of Design, an imprint of Watson-Guptill Publications, New York.

Vukobratovic, M. and Borovac, B. 2004. Zero moment point – thirty-five years of its life. *International Journal of Humanoid Robotics* 1(1):157–173.

Vukobratovic, M. and Juricic, D. 1969. Contributions to the synthesis of biped gait. *IEEE Transactions on Biomedical Engineering* 16:1–6.

Vukobratovic, M. and Stepanenko, Y. U. 1973. Mathematical models of general anthropomorphic systems. *Mathemat-*

ical Biosciences 17:191–242.

Vukobratovic, M., Frank, A., and Juricic, D. 1970. On the stability of biped locomotion. *IEEE Transactions on Biomedical Engineering* 17(1):25–36.

Winter, D. A. 1990. *Biomechanics and Motor Control of Human Movement*, Wiley, New York.

Witkin, A. and Kass, M. 1988. Spacetime constraints. *Computer Graphics (SIGGRAPH '88 Proceedings)*, J. Dill, editor, Vol. 22, pp. 159–168.

Wollherr, D., Buss, M., Hardt, M., and von Stryk, O. 2003. Research and development toward an autonomous biped walking robot. *Proceedings of the IEEE/ASME International Conference on Advanced Intelligent Mechatronics (AIM),* Kobe, Japan, pp. 968–973.

Wright, D. B., Desai, S. M., and Henderson, W. H. 1964. Action of the subtalar and ankle-joint complex during the stance phase of walking. *Journal of. Bone Joint Surgery* 46-A:361.

Yamaguchi, J., Takanishi, A., and Kato, I. 1993. Development of a biped walking robot compensation for three-axis moment by trunk motion. *Proceedings of the IEEE/RSJ International Conference on Intelligent Robots and Systems*, Yokohama, Japan.

Yamaguchi, J., Soga, E., Inoue, S., and Takanishi, A., 1999. Development of a bipedal humanoid robot – control method of whole-body cooperative dynamic biped walking. *Proceedings of the IEEE International Conference on Robotics and Automation*, Detroit, MI, pp. 368–374.